Next Materials 8 (2025) 100729

Contents lists available at ScienceDirect

Next Materials

journal homepage: www.sciencedirect.com/journal/next-materials

Research article

Assessment of microstructural architecture and mechanical properties of levonorgestrel loaded PCL/PLGA/HA nanofibers

Peace-OfonAbasi O. Bassey [a,1], Bukola A. Oseni [a,2], Deborah A. Ogundemuren [a,3], Karamot O. Oyediran [a,4], Evans N. Ekeji [b,5], Dimitrios Tsamos [c,6], Alkiviadis Tsamis [c,d,7], Alexandros E. Tsouknidas [c,8], Bryan C. Okwuba [a,9], David A. Vorp [e,10], Samson A. Adeosun [f,11], Margaret O. Ilomuanya [a,g,12,*]

[a] Department of Pharmaceutics and Pharmaceutical Technology, Faculty of Pharmacy, University of Lagos, Lagos, Nigeria
[b] Department of Pharmaceutical Chemistry, Faculty of Pharmacy, University of Lagos, Nigeria
[c] Department of Mechanical Engineering, University of Western Macedonia, Kozani 50100, Greece
[d] School of Engineering, University of Leicester, Leicester LE1 7RH, United Kingdom
[e] Departments of Bioengineering, Surgery, Cardiothoracic Surgery, Mechanical Engineering & Materials Science, Chemical and Petroleum Engineering, McGowan Institute for Regenerative Medicine, Clinical & Translational Sciences Institute, University of Pittsburgh, Pittsburgh, PA 15261, USA
[f] Department of Metallurgical and Materials Engineering, Faculty of Engineering, University of Lagos, Lagos, Nigeria
[g] MEDAFRICA GMP Laboratory, Faculty of Pharmacy, University of Lagos, Nigeria

ARTICLE INFO

Keywords:
Sodium Cocoamphoacetate (CAP)
Polycaprolactone (PCL)
Poly (lactic-co-glycolic acid) (PLGA)
Hyaluronic Acid (HA)
Levonorgestrel (LNG)
Nanofibers
Mechanical Properties

ABSTRACT

The combination of Polycaprolactone (PCL), Poly (lactic-co-glycolic acid) (PLGA), and hyaluronic acid (HA) in nanofiber formulations offers a synergistic approach for the development of advanced biomaterials. Understanding the inherent limitations of individual polymers and the modification of key parameters in nanofiber production is crucial for fabricating composite electrospun fibers especially for the purpose of contraception. This study investigates the microstructural characteristics, and mechanical properties of PCL/PLGA/HA loaded Levonorgestrel (LNG) nanofibers for contraception. PCL, PLGA, and HA were mixed in suitable diluents at a ratio of 3:2:1. Levonorgestrel was added to the polymer blend. PCL/PLGA/HA was electrospun with surfactant sodium cocoamphoacetate (CAP) and an outer layer of HA was electrosprayed in the same proportion as stated above. Eight nanofiber samples were fabricated, each varying in collector type, presence of LNG, and additional treatments with CAP. The mean diameter of samples ranged from 6.28 ± 0.27 pix to 5.38 ± 0.07 pix. The tensile strength, Young's modulus and elongation at break were also determined. This study showed the relationship between formulation and processing parameters and the resulting fiber characteristics via image-based analysis and mechanical testing, highlighting the potential for precise control over nanofiber properties for tailoring nanofiber mats for delivery of Levonorgestrel in contraception.

* Corresponding author at: Department of Pharmaceutics and Pharmaceutical Technology, Faculty of Pharmacy, University of Lagos, Lagos, Nigeria.
E-mail address: milomuanya@unilag.edu.ng (M.O. Ilomuanya).
[1] https://orcid.org/0009-0001-5419-8281
[2] https://orcid.org/0000-0003-4306-7101
[3] https://orcid.org/0009-0003-7799-7152
[4] https://orcid.org/0000-0003-2246-2364
[5] https://orcid.org/0000-0002-5939-8194
[6] https://orcid.org/0000-0002-8107-4778
[7] https://orcid.org/0000-0001-8101-3302
[8] https://orcid.org/0000-0001-7339-3165
[9] https://orcid.org/0009-0002-9311-2804
[10] https://orcid.org/0000-0002-6467-2151
[11] https://orcid.org/0000-0001-9847-7592
[12] https://orcid.org/0000-0001-8819-1937

https://doi.org/10.1016/j.nxmate.2025.100729
Received 13 November 2024; Received in revised form 26 April 2025; Accepted 14 May 2025
Available online 20 May 2025

1. Introduction

Nanofibers have emerged as a pivotal component in the advancement of biomedical applications due to their unique structural and functional properties. These fibers are characterized by high surface area-to-volume ratio, adequate porosity, ability to mimic the extracellular matrix, and have shown immense potential in areas such as drug delivery, wound healing, and tissue engineering [1,2]. The high surface area facilitates high drug loading and controlled release [3,4] while the porous structure supports cell growth and tissue integration, making nanofibers particularly well-suited for biomedical uses [2,3].

These nanofibers have significantly been employed for the delivery of doxorubicin (dox) using carbon nanotube (CNT) nanofibers. The dox was chemically incorporated into the CNT nanofibers, achieving a high encapsulation efficiency of 83.7 %. Additionally, a PLGA polymer solution was combined with dox particles in three distinct ratios to produce suitable nanofibers via electrospinning [5]. Modified forms of several therapeutic agents, including proteins, peptides, antibodies, and small molecular pharmaceuticals, have been integrated into the nanofibers to facilitate targeted delivery and achieve more favorable outcomes with effective therapeutic activity [6]. Electrospun nanofibers integrating the biocompatibility of PVA, the bioactivity of keratin and CoQ10, and the antibacterial efficacy of mupirocin have been successfully produced as a novel approach for effective wound treatment [7]. Mucoadhesive electrospun nanofibers was developed addressing drug-resistant *P. aeruginosa* wound infections in an animal model by the incorporation of MDR-specific phage Pϕ-Mi-Pa [8]. Electrospun nanofibers for the management of bacterial vaginosis by the inclusion of a surfactant, metronidazole, and *Lactobacilli spp.* have been developed [9].

Polycaprolactone (PCL) is a biocompatible and biodegradable polyester that has gained significant attention in biomedical applications. Its slow degradation rate makes it an ideal candidate for long-term implants and drug delivery systems [10,11]. Poly (lactic-co-glycolic acid) has been utilized due to its superior biocompatibility, customizable biodegradability, tunable degradation rate, and excellent mechanical qualities. PLGA's degradation rate can be tailored by adjusting the ratio of lactic acid to glycolic acid, allowing for controlled drug release profiles [12,13].

Hyaluronic Acid (HA) is a naturally occurring polysaccharide found in the extracellular matrix of connective tissues [14,15]. Its hydrophilicity, biocompatibility and mucoadhesion makes it an excellent material for biomedical applications especially in the field of vaginal drug delivery [16]. HA's ability to promote cell adhesion, proliferation, and differentiation is crucial for developing nanofibers that facilitate tissue repair and regeneration [17,18]. The integration of PCL, PLGA, and HA in nanofiber formulations offers a synergistic approach to developing advanced biomaterials. These composite nanofibers can combine the mechanical strength of PCL, the tunable degradation of PLGA, and the biological activity of HA, creating multifunctional nanofibers tailored for specific biomedical applications [11,14,19] and in specific, contraception.

Levonorgestrel is a synthetic progestin, a derivative of the natural hormone progesterone, widely utilized in various contraceptive methods such as oral contraceptives and intrauterine devices (IUDs) [20]. It has been incorporated into various formulations, such as the levonorgestrel-releasing intrauterine system (LNG-IUS), which provides a sustained release of the hormone directly into the uterine cavity, thus enhancing contraceptive efficacy [21]. Furthermore, levonorgestrel is also available in oral form as an emergency contraceptive pill (ECP), which can be taken after unprotected intercourse to prevent pregnancy [22]. The mechanism of action of LNG primarily involves the inhibition of ovulation, changes in cervical mucus, prevention or delay of ovulation reducing the likelihood of fertilization [23,24] and creation of an unfavorable environment for implantation by modifying the endometrial lining preventing a fertilized eggs from successfully implanting [25].

Scanning electron microscopy has been observed to be a suitable image-based analysis tool to extract micro-architectural features and has been created to accurately characterize the structure of engineered-tissue fiber networks. This tool utilizes a Delaunay-network skeleton and image-gradient information. The identified and measured micro-architectural characteristics encompass the distribution of fiber angles, connectedness of nodes, density of spatial intersections, and diameter of fibers [26,27].

While electrospun nanofibers have shown great potential for localized drug delivery, particularly for Levonorgestrel (LNG), significant gaps remain in understanding how the microstructural properties of these fibers influence their mechanical characteristics and drug release profiles. Current research has primarily focused on the general advantages of electrospun nanofibers, such as their high surface area and tunable porosity, but there is a lack of detailed studies correlating microstructural and mechanical properties with LNG-loaded fiber performance. Understanding these relationships is essential for optimizing the design of nanofibers that can withstand the mechanical stresses encountered in biological environments while effectively delivering LNG. Maintaining the mechanical integrity of a mucoadhesive formulation is crucial when it is intended to interact with mucosal tissue and nanofibers exhibit distinctive characteristics, particularly in terms of outstanding mechanical strength and flexibility which supports this [28]. This has been reported for PCL [9] and PLGA [29]. The formulations of nanofibers intended for mucoadhesion must exhibit significant pliability, as formulations with reduced flexibility are recognized to induce irritation at the administration site. Hence the need to understand the influence of LNG loading on mechanical characteristics of nanofibers.

There have been undesirable side effects associated with available contraceptives and long duration of residual hormonal effects after discontinuation. This limits the desirability and acceptance of contraceptive options, often leading to dissatisfaction and discontinuation of use. On demand release mechanisms are needed targeting the vagina to reduce the burden of systemic hormonal delivery and electrospun nanofibers serve as a platform. These nanofibers possess sufficient degradability that facilitates clearance, reducing the duration required for the restoration of fertility and mitigating related side effects. The utilization of the vagina as a delivery route will provide dose reduction, hence diminishing the negative effects associated with alternative dosage formulations and routes of administration.

This study aims to assess the microstructural and mechanical properties of PCL/PLGA/HA nanofibers loaded with LNG using SEM which will serve as a platform for contraception. This hybrid tripolymeric system has not been used in LNG delivery. The use of PCL will improve the biocompatibility and mechanical robustness of the electrospun nanofibers while PLGA will enhance and provide adjustable biodegradability. The incorporation of HA will facilitate its adhesion to the mucosal membranes of the vagina. The enzymatic activity of hyaluronidase, which is present in seminal fluid, facilitates the degradation of the hyaluronic acid constituent in the polymer matrix, thereby enabling the stimuli responsive release of LNG. Specifically, the study investigates how the presence or absence of CAP, the use of different collector types, and the incorporation of LNG influence nanofiber characteristics. Comprehensively analyzing these variables, the study provides an understanding of how they modify fiber diameter, tensile strength, and porosity. It assesses how these characteristics also influence mechanical strength, degradation and drug release. Understanding these microstructural properties can lead to more efficient drug encapsulation and release mechanisms of LNG for vaginal drug delivery. The outcomes will contribute towards developing biomaterials for targeted and stimuli sensitive drug delivery particularly in the field of reproductive health [30,31].

2. Materials and methods

2.1. Materials

Polycaprolactone with average MW of 50 kDa (Energy Chemicals Inc., Shanghai), poly (lactic-co-glycolic acid) PLGA 50/50 COOH (Mw: 31K-57k), levonorgestrel (LNG) (Mw: 312.45, CAS No 797–63–7) (Macklin Biochemical Co, Ltd., China), sodium hyaluronate (HA) (Mw:1200 kDa, CAS No. 9067–32–7) (Nanjing Pars Biochem Co., Ltd., China), deionized water, chloroform (CAS No. 67–66–3) (Molychem, India), ethanol (CAS No. 64–17–5) (Honeywell, Germany). The reagents were of analytical grade and no further purification was needed before their use.

2.2. Methods

2.2.1. Electrospinning process

The polymer solutions were prepared by dissolving 20 g of PCL in a solvent system of chloroform: ethanol (1:1). This was done at room temperature and left overnight for complete dissolution [9]. 0.5 g of PLGA was dissolved in 100 mL of chloroform with magnetic stirring for 2 h. 0.5 g of HA was dissolved in deionized water and ethanol solvent system (9:1) with magnetic stirring for 4 h at room temperature. PCL/PLGA/HA was then mixed in the ratio of 3:2:1. Levonorgestrel (1.96 % w/w) was dissolved in PCL and then added to the polymer blend and stirred for 3 h without heat at 150 rpm.

Fiber mats were electrospun with PCL/PLGA/HA and surfactant sodium cocoamphoacetate (CAP) and electrosprayed with an outer layer of HA in the same proportion as stated above. The study involved eight distinct nanofiber samples, each varying in collector type, presence of LNG, and additional treatments with CAP. PE1 used a plate collector without LNG, while PE2 used a wire collector without LNG. PE3 incorporated 1.96 %w/w of LNG using a plate collector, and PE4 used a wire collector with 1.96 %w/w LNG. For samples PE5 to PE8, an outer coating of HA was applied in addition to the use of CAP as a surfactant. Specifically, PE5 matched PE1's conditions, PE6 matched PE2's, PE7 matched PE3's, and PE8 matched PE4's, but all included the surfactant and HA coating (Table 1 below).

2.2.2. Morphological characterization

Scanning electron microscopy (JSM-6610 Scanning electron microscope by JEOL, USA) was used to analyze the morphological structure of all nanofibers. The samples were divided into small (5 mm × 5 mm) pieces and sputtered with gold for 2 minutes. At 15 kV, 2.8 kx and 40.0 kx magnifications were used to obtain each image.

2.2.3. Processing of images

2.2.3.1. Equalization of intensity and extraction of fibers. The fiber edges of the image were preserved via image smoothing using the MATLAB function for median filtering (3 ×3 window, MF medfilt2) contrast-enhanced utilizing contrast-limited adaptive histogram equalization (3 ×3 window, MF adapthisteq) and histogram adjustment (MF imadjust), where 1 % of the image was subjected to saturation at the periphery. Image adjustment was done to balance the noise and intensity levels between inputs and to ensure that the maximum available dynamic range was employed. Noise and background information was diminished, enhanced fibrous information was carried out using multiscale vessel-enhancement filtering [26]. The Frangi algorithm analyzed intensity gradients, searching out tube-like vessels. Projection of the components occurred via the filter which in turn led to low yield of non-tube-like information. Image threshold-filtering was done using a value of 0.4 as the cutoff intensity by creating a binary, black and white image and segmenting the fiber information from the background. The value 0.4, fixed for all images, was qualitatively determined to minimize fiber diameter deviations from the grayscale to binary image. The complement of the binary image was subjected to a Euclidean-distance transform (MF bwdist) to measure the distance from every pixel within the fibers to the fiber extreme. Ridges in the distance-transformed image which served to mark an approximate epicenter of the best of the well-defined fibers were put in place by doing a watershed -transform (MF watershed). This image served as a mask on the distance-transformed image to bring about initial fiber diameter values. A representative fiber diameter (FD) was obtained from the median of the fiber diameter values. As a result of artifacts present at the edges of the image from the filtering techniques, FD-pixels were cropped from the four edges of the image which resulted in a binary, black and white (BW) image.

2.2.3.2. Fiber skeletonization and intersection identification. In order to smoothen the edges of the fiber and remove the small holes and fiber fragments that might have been in the background or incomplete information, the BW image was subjected to a series of morphological operations First, the BW image was eroded (structuring element (SE) disk radius = FD/8, MF imerode), then dilated (SE disk radius = FD/4, MF imdilate), then eroded again (SE disk radius = FD/8). The image was eroded before dilation to allow for smoothing without closing small gaps between fibers. The original size of the fibers was reinstated to their original sizes with smoother edges by re-erosion. The resulting image was morphologically thinned (MF bwmorph ('thin')) to form a 1-pixel thick representation of the fibers. Segments with areas smaller than 2 x FD were considered negligible fragments and removed (MF bwareaopen). The skeleton was dilated (SE disk radius = FD/2) and holes smaller than π x (FD/2) ^{2} were removed. Small branches were pruned from the skeleton and neighboring intersections were merged by dilating the intersection points (SE disk radius = FD + FD/2) and rethinning the image. The resulting image was a 1-pixel thick fiber skeleton (FS). An Euclidean-distance transform was performed on the BW image to calculate the fiber diameter distribution in the image. The resultant image was then masked using the FS to isolate the fiber radii values associated with the FS.

2.2.3.3. Analysis of tortuosity and orientation of electrospun nanofibers. To examine the tortuosity and orientation of the fibers, the junctions in the fiber structure (FS) were eliminated by inducing dilation at the places of intersection (using a square structuring element with a length of 3). This process produced a segmented skeleton (SS) consisting of separate fiber segments. The SS enabled the determination of discrete fiber segment endpoints, essential for the computation of fiber tortuosity. Tortuosity is the quotient obtained by dividing the length of a segment by the vertical distance between its ends [32]. Sampling was conducted at regular intervals of FD pixels throughout the length of each section of the SS. The orientation of the sub-segments was established by measuring the angle formed by the tangent line connecting the initial and final positions of each sub-segment. The FD was chosen as the

Table 1
Formulation design for PCL/PLGA/HA electrospinning solutions.

Sample	PCL (% w/v)	PLGA (%w/v)	HA (% w/v)	LNG (% w/w)	Voltage	Plate Collector	Wire collector (750 rpm)
PE1	20	0.5	0.5	-	25	*	-
PE2	20	0.5	0.5	-	25	-	*
PE3	20	0.5	0.5	1.96	25	*	-
PE4	20	0.5	0.5	1.96	30	-	*
PE5*	20	0.5	0.5	-	25	*	-
PE6*	20	0.5	0.5	-	25		*
PE7*	20	0.5	0.5	1.96	25	*	-
PE8*	20	0.5	0.5	1.96	30	-	*

* corresponds to the collector selection

sample distance because it achieved a compromise between the need for angular accuracy and the capability to detect fiber tortuosity (FT).

2.2.3.4. Analysis of concentration, porosity, and intersection density of electrospun nanofibers. A programmatically chosen region of interest inside the picture was used to facilitate area-based computations for concentration, porosity, and intersection density, hence mitigating human bias. The total value of each row and column in the BW picture was calculated, and the image was trimmed at the four corners above a predetermined threshold. Following the cropping, the picture was partitioned into frames of 100 × 100 pixels. The concentration, which is the proportion of white pixels to the total pixels, was then computed for each frame [20]. Concentrated regions were defined as frames consisting of concentrations within ± 1 standard deviation from the average of the picture. The measurements of fiber concentration, porosity (the proportion of black pixels to the total pixels), and intersection density (the ratio of intersection points to the size of the region of interest) were performed using these specific regions.

2.2.4. Mechanical characterization

2.2.4.1. Tensile strength. Tensile strength was measured using a universal testing machine (Instron Model 5567) equipped with a 10 N load cell. The nanofibers were cut into rectangular strips (10 mm×50 mm) and mounted on the testing machine with a gauge length of 30 mm. Samples with and without LNG, sprayed with Hyaluronic Acid (HA), and with different collector types (plate and wire) were included to evaluate the effects of these variables. The tests were conducted at a constant crosshead speed of 5 mm/min until the samples failed. The test was carried out in triplicates. Tensile strength (σ_t) was calculated using Eq. 1:

$$\sigma_t = \frac{\text{Force(N)}}{\text{Area(mm}^2\text{)}} \ldots\ldots\ldots \quad (1)$$

2.2.4.2. Young's modulus. Young's modulus (E) is a measure of the stiffness of the nanofibers and was determined from the slope of the initial linear portion of the stress-strain curve obtained from the tensile tests. Samples with and without LNG, sprayed with HA, and with different collector types were included to evaluate the effects of these variables. This was carried out in triplicates. The stress (σ) and strain (ϵ) were calculated as follows:

$$\text{Stress}(\sigma) = \frac{\text{Force(N)}}{\text{Area(mm}^2\text{)}} \ldots\ldots\ldots \quad (2)$$

$$\text{Strain}(\epsilon) = \frac{\text{L}_f - \text{L}_0\text{(mm)}}{\text{L}_0 \quad \text{(mm)}} \ldots\ldots\ldots \quad (3)$$

where L_f = final Length, L_0 = Initial Length

$$\text{Young's Modulus} = \frac{\sigma}{\epsilon} \ldots\ldots\ldots \quad (4)$$

2.2.4.3. Elongation at break (%). Elongation at break (ϵ_b) is a measure of the ductility of the nanofibers and is expressed as the percentage increase in length at the point of fracture. It was calculated using the formula:

$$\text{Elongation at break}(\epsilon_b) = \left(\frac{\text{L}_f - \text{L}_0}{\text{L}_0}\right)\text{x100} \ldots\ldots \quad (5)$$

Where L_f = Final length, and L_0 = original length.

This was carried out in triplicates.

2.3. In vitro LNG release

The release of LNG was assessed in the presence of seminal fluid (SF) to examine its impact on the polymer matrix of the nanofibers. Simulated vaginal fluid (SVF) was combined with seminal fluid (SF) obtained from a donor in a ratio of 1:4, respectively considering the typical volumes of male ejaculate and human vaginal fluid. The pH of the mixture was subsequently adjusted to 7.1 utilizing 0.1 N Hydrochloric Acid (HCl) [33]. 10 mg of electrospun scaffold was suspended in 3 mL of the mixture and subsequently dispersed into Franz diffusion cells. The scaffold was maintained on a membrane in a 25 mL release medium (SVF, pH 4.2), and deposited in an agitating water bath at a constant temperature of 37 ∘C. At specified time intervals of 0, 1/2, 1, 3, 6, 24, 48, and 72 hours, 2 mL of the sample was extracted from the release medium and subsequently transferred into a sterile sample vial. At each withdrawal interval, an equivalent volume of the release medium was substituted to maintain sink conditions. Absorbance was taken at 240 nm using ultraviolet (UV) spectrophotometer (Shimadzu UV-1601 PC, Japan) to determine the quantity of LNG releaseed from the polymer matrix in the presence of seminal fluid. The cumulative percentage of LNG permeating the membrane was graphically represented as a function of time [24]. This was carried out in triplicates.

2.4. Assessment of Entrapment Efficiency (EE), drug loading and fiber yield

The drug entrapment efficiency of the electrospun nanofibers was evaluated by dissolving 10 mg of the electrospun nanofibers in 10 mL of ethanol for a duration of 5 minutes, utilizing a magnetic stirrer. The quantity of LNG was ascertained using a UV/VIS spectrophotometer (Shimadzu UV-1601 PC, Japan) at a wavelength of 240 nm. The quantification was conducted by utilizing a pre-established standard curve as a reference. The experiment was conducted three times, and the results were analyzed to determine the mean value along with the associated standard deviation. The EE %, drug loading and fiber yield was assessed using the equations below: [34]

$$\text{EE\%} = \frac{\text{Amount of drug in NFs}}{\text{Drug initially added}} \times 100 \ldots\ldots\ldots \quad (6)$$

$$\text{Drug loading} = \frac{\text{Weight of drug in fiber}}{\text{Weight of the fiber taken}} \times 100 \ldots\ldots \quad (7)$$

$$\text{Fiber yield} = \frac{\textit{Total mass of electrospun fibers}}{\text{Calculated mass of solids in solution added in the syringe}} \times 100 \ldots\ldots \quad (8)$$

2.5. Biodegradation studies in simulated vaginal fluid (SVF)/ Seminal Fluid (SF)

Electrospun nanofibers with a diameter of 1.5 cm were immersed in a mixture of SVF/SF in a ratio of 1:4. The pH of the solution was adjusted to 7.1 using 0.1 N HCl, and the nanofibers were maintained in a controlled environment for a duration of three days at ambient temperature. At designated intervals, the electrospun nanofibers were removed, subjected to cleansing with sterile distilled water, air-dried, and subsequently weighed. The composition of the solution was changed periodically throughout the analysis. This process was carried out in triplicates [35].

$$\text{Weight loss\%} = \frac{W_i - W_f}{W_i} \times 100 \ldots\ldots\ldots\ldots \quad (9)$$

W_i = *Initial weight* W_f = *final weight*

2.6. Statistical analysis

Statistical analysis for this study was conducted using GraphPad Prism and OriginPro software. Descriptive statistics were calculated to

summarize the data, and normality was assessed using the Shapiro-Wilk test. One-way ANOVA was performed to identify significant differences among the nanofiber samples, with Tukey's post-hoc test used for pairwise comparisons. Statistically significant differences between formulations were indicated with asterisks (*P ≤ 0.05, **P ≤ 0.01, ***P ≤ 0.001, ****P ≤ 0.0001). OriginPro software was utilized for graphical representation, including bar graphs and scatter plots, with error bars and confidence intervals illustrating variability and precision.

3. Results/discussion

This study assessed the microstructural architecture and mechanical properties of electrospun nanofibers composed of PCL/PLGA/HAloaded with LNG. The aim was to optimize the fiber characteristics for delivery of a contraceptive using an image analysis tool and mechanical testing. This has the benefit of analyzing fiber structure at a certain depth without requiring fiber preprocessing. The image-analysis tool utilized advanced image-processing techniques to effectively address the challenges of noise, saturation, and complexity to accurately define crucial micro-architectural features. Through analyzing the different polymer blends and loading conditions, the influence of these variables on fiber morphology, mechanical strength, and overall performance could be understood.

3.1. Morphological properties

The SEM images illustrated revealed fibers with varying average diameters and beading characteristics (Fig. 1), representative histograms for diameter distribution were displayed in Figs. 2a and 2b. PE1 fibers had a representative average diameter of 6.59 pix and did not show any beading. In contrast, PE2 fibers, with an average diameter of 5.92 pix, exhibited spherical beading ranging from 1 to 10 pix). PE3 fibers had a representative average diameter of 5.83 pix as seen in the corresponding histogram (Fig. 2a) and showed oval-shaped beading with an average diameter of 3.50 pix. PE4 fibers, with an average diameter of 5.42 pix, also displayed spherical beading with diameters between 0.4 and 4.4 pix. PE5 fibers, similar to PE1, did not exhibit any beading and had an average diameter of 6.55 pix. PE6 fibers had an average diameter of 5.78 pix and spherical beading with a diameter of 1.2 pix. PE7 fibers, averaging 6.05 pix in diameter, displayed spherical beading ranging from 0.3 to 1.9 pix. PE8 fibers, with an average diameter of 5.53 pix, exhibited spherical beading with diameters between 0.4 and 2.8 pix.

3.1.1. Intersection density (%) of electrospun fibers

The Intersection density details the rate at which fibers intersect or cross each other within a specified region or volume of the nanofiber mat. Electrospun fibers with a greater intersection density generally exhibits a more densely packed structure, enhancing encapsulation of drugs in fibrous matrix and can lead to a more intricate and convoluted route for the drug release through the matrix. This can be employed for sustained release while fibers with lower intersection density may have larger pores and fewer encapsulation sites resulting in reduced drug loading capacity, less efficient encapsulation but increase drug diffusion through matrix which could be of interest for burst and immediate release effect. Fig. 3A shows the difference in the intersection densities between the formulations with PE6 (0.35 ± 0.09 %) having a significantly higher intersection density compared to all the formulations.

Regarding the impact of the CAP (Fig. 4) and an outer coating of HA on the intersection densities of fibers in various formulations, in the first comparison between PE5 and PE1, PE5 shows a significantly higher intersection density ($p < 0.05$). PE6 and PE2 also reveal a significantly higher intersection density for PE6 ($p < 0.05$). Similarly, between PE3 and PE7, PE7 demonstrates a significantly higher intersection density ($p < 0.05$). Lastly, PE8 and PE4 continue this trend, with PE8 having a significantly higher intersection density ($p < 0.05$). The effect of the collector type on the intersection density was seen to be significantly higher in PE2 (0.06 %) compared to PE1 (0.12 %) ($p = 0.0067$). Similarly, PE4 (0.34 %) showed significantly higher value compared to PE3 (0.15 %) ($p = 0.000065$) (Fig. 5). Moreover, the addition of LNG significantly increased intersection density in PE4 (0.34 %) compared to PE2 (0.06 %) ($p = 0.000001$). For PE7 (0.23 %) compared to PE5 (0.33 %), Intersection Density decreased significantly ($p = 0.019$ %) (Fig. 6). The study found significant variations in intersection density across different formulations, with PE4, PE5, and PE6 showing higher densities compared to PE1, PE2, and PE3. This aligns with the findings of Conte *et al.*[36], who reported that fiber density correlates with mechanical properties of nanofiber mats. While Conte *et al.* observed that Young's modulus reduced as fiber density increased, our study revealed a more complex relationship. For instance, PE3 (plate collector with LNG) showed a significantly higher Young's modulus (28.66 ± 20.29 MPa) compared to PE1 (5.02 ± 4.40 MPa), despite having a

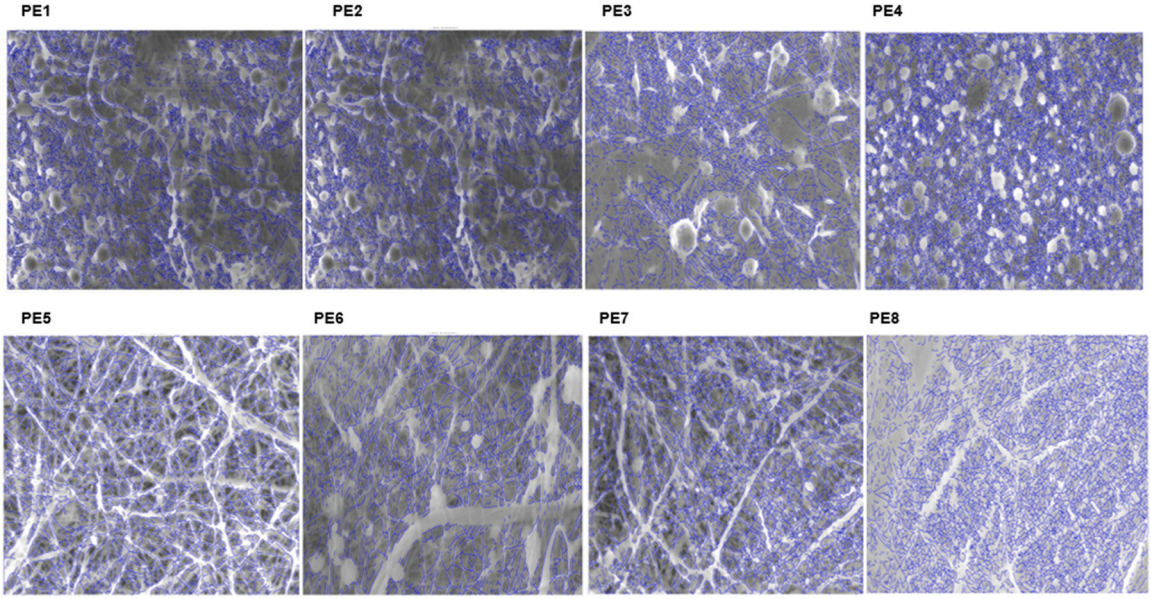

Fig. 1. Scanning electron microscopy of electrospun fibers showing the fiber skeleton.

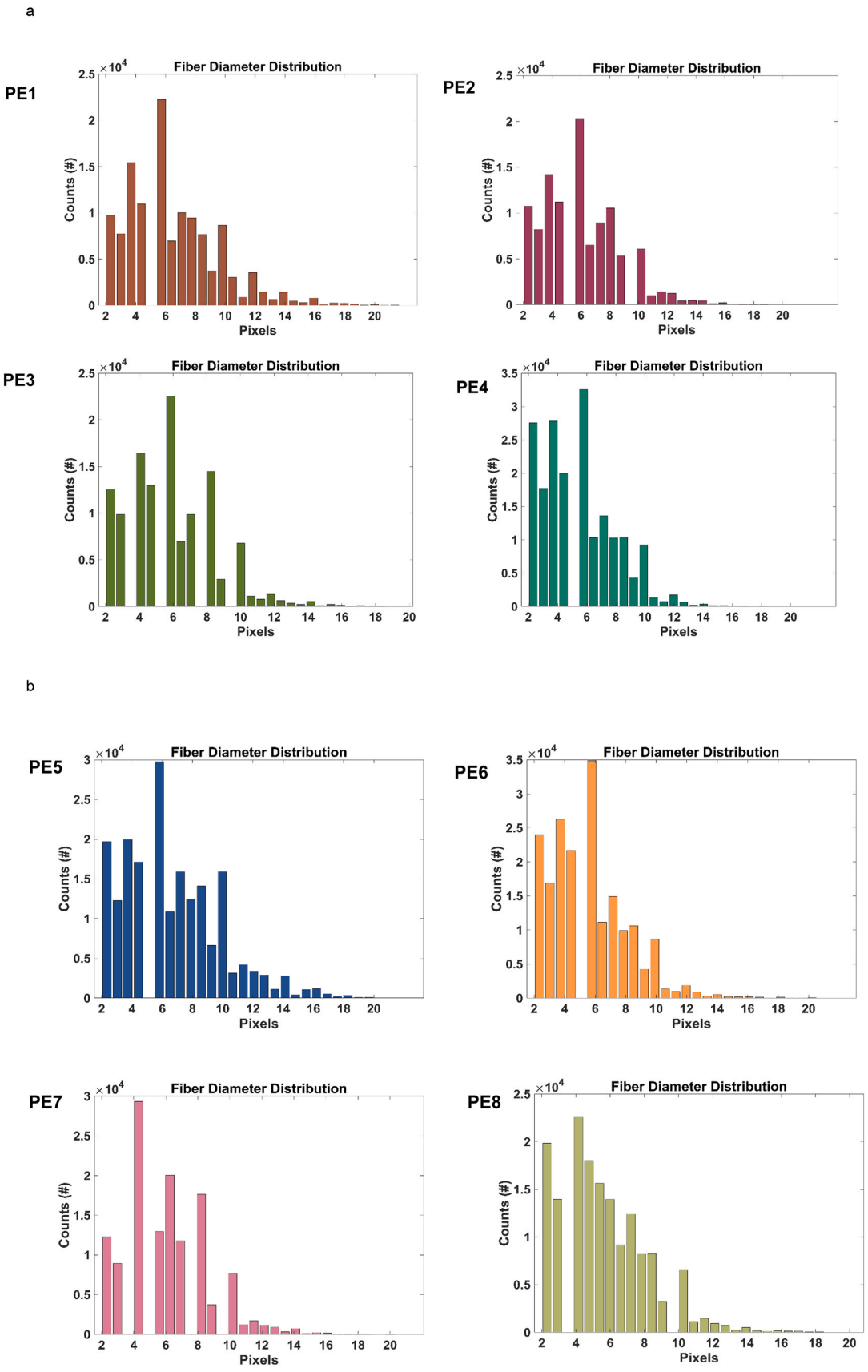

Fig. 2. **a**. Fiber diameter distributions of electrospun nanofibers. **b.** Fiber diameter distributions of electrospun fibers.

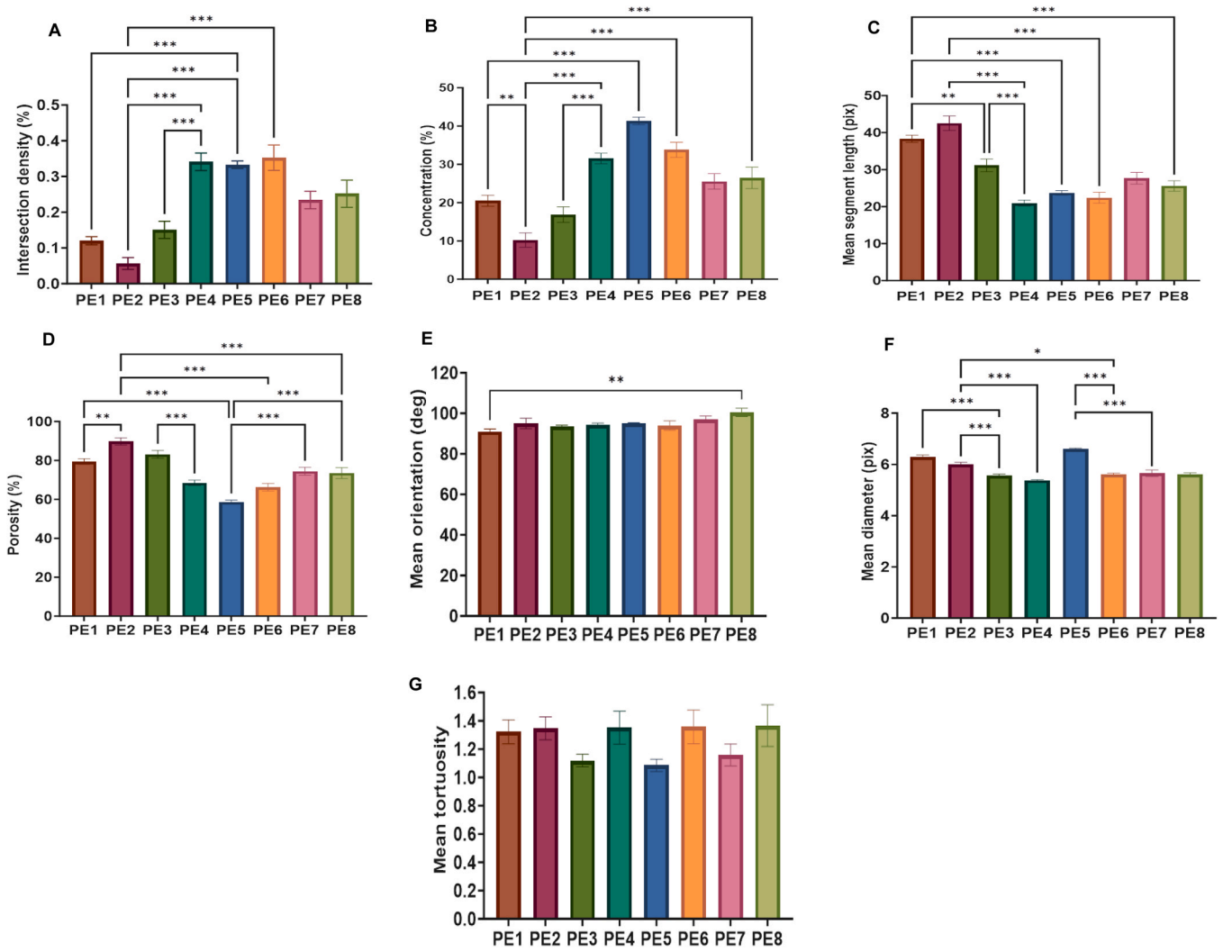

Fig. 3. A) Intersection Density (%) B) Concentration (%) C) Mean segment length (pix) D) Porosity (%) E) Mean Orientation (deg) (%) F) Mean Diameter (pix) G) Mean Tortuosity of electrospun fibers. *(Statistically significant differences are indicated with asterisks. *P < =0.05, **p < = 0.01, ***p < = 0.001).*

lower intersection density. This suggests that factors beyond intersection density, such as flow rate, voltage, collector distance as well as the physical and chemical properties of the polymer.

The presence of LNG could also have an effect in determining mechanical properties of the fibers. The effect of collector type on intersection density (Fig. 5), where the wire collector (PE2 and PE4) resulted in higher densities compared to the plate collector (PE1 and PE3), introduces a new perspective and points to the possibility that the collector type could be an important parameter in controlling fiber arrangement and influencing mat properties, a concept that merits further investigation. The jet motion during electrospinning is influenced by the fiber collection shape, thereby affecting the electric field intensity distribution and fiber properties [37]. The increased intersection density in formulations with CAP and HA coating suggests that these may influence fiber arrangement and interaction. This observation is particularly interesting when compared to the findings of Stachewicz *et al.* [38], who noted that solution interactions with electrospun fiber mats can influence mechanical properties in nanocomposites.

3.1.2. Concentration of electrospun fibers (%)

The concentration of the electrospun fibers is seen in Fig. 3B with PE5 (41.33 ± 2.19 %) showing a significantly higher value among all the comparisons. The addition of CAP, along with an outer coating of HA, greatly affected the concentration of the fibers. Comparing PE5 to PE1, PE5 showed a significantly higher concentration ($p < 0.001$) (Fig. 4). Also, PE6 (with surfactant and HA) had a higher concentration at the intersections than PE2 ($p < 0.001$). PE7 also exhibited a significantly higher concentration compared to PE2 ($p < 0.001$) and PE3 ($p < 0.001$). Finally, PE8 showed a significantly higher concentration than PE2 ($p < 0.001$) and PE3 ($p = 0.025$).

Also, the effect of the collector type on the concentration of the intersection of the fibers showed to be lower in PE2 compared to PE1 ($p = 0.000540$). PE4 showed a significantly higher concentration compared to PE3 ($p = 0.000030$). There was an increased concentration upon the addition of LNG in PE4 compared to PE2 ($p < 0.0001$). The concentration of the fiber also decreased significantly in PE7 (25.55) compared to PE5 ($p = 0.000503$) (Fig. 6).

The findings of this study showed significant differences in the concentration of the fibers among the different fiber preparations which appear to be influenced by factors such as the addition of active ingredients, coatings, and collector types. Considering Rambabu *et al.*'s study [39] which reported that the morphology and properties of nanofibers can be significantly affected by chemical treatments and processing methods. This substantiates the finding of this study on the addition of CAP and HA coating similarly affecting concentration of the fibers, which could potentially influence the overall structure and properties of the nanofiber mats. Moreover, Conte *et al.*'s [36] study found that increasing fiber density led to increased ultimate tensile

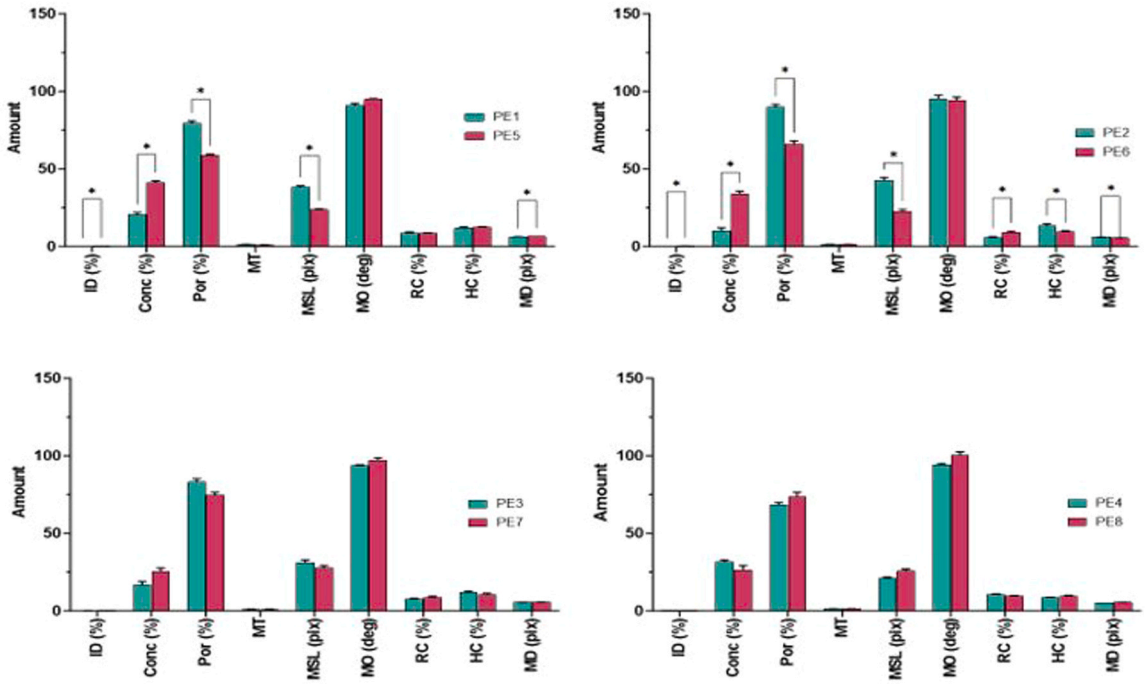

Fig. 4. Effect of surfactant (CAP) on morphological properties of electrospun fibers. **ID = Intersection Density, Conc = Concentration, Por = Porosity, MT= Mean Tortuosity, MSL= Mean Segment Length, MO= Mean Orientation, RC= Radial Count, HC= Horizontal Count, MD = Mean Diameter.**

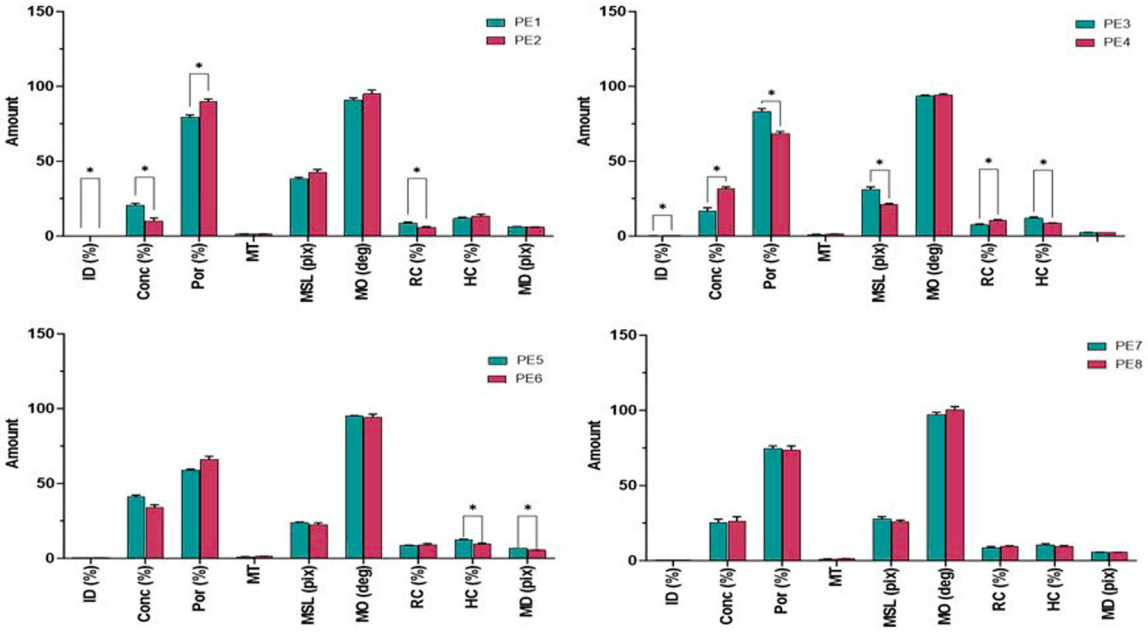

Fig. 5. Effect of collector type on morphological properties of electrospun fibers. **ID = Intersection Density, Conc = Concentration, Por = Porosity, MT= Mean Tortuosity, MSL= Mean Segment Length, MO= Mean Orientation, RC= Radial Count, HC= Horizontal Count, MD = Mean Diameter**.

strength and toughness, but decreased Young's modulus. This study's findings on fiber concentrations could be related to fiber density, as higher intersection concentrations might indicate higher overall fiber density in the mat. This suggests that the samples with higher fiber concentrations (e.g., PE5, PE6) might exhibit different mechanical properties compared to those with lower concentrations (e.g., PE2). It has also been noted that proper impregnation of the nanofiber network with a matrix material led to improved mechanical properties [38]. This is in line with the results of this study where the addition of CAP and HA coating, which increased concentration of electrospun fibers, might have affected the interaction between fibers and any matrix material, potentially influencing the mechanical properties of the resulting composites. Meanwhile, the study's findings on the effect of collector type on fiber intersection concentration (e.g., lower in PE2 compared to PE1) are parallel with observations from Amiraliyan *et al.* [40], which noted that collector characteristics in their study significantly affected the morphology of the fibers in this case including the intersection concentrations. The increase in fiber intersection concentration upon addition of LNG (comparing PE4 to PE2) indicates that the incorporation of active ingredients can significantly alter the fiber mat structure. This

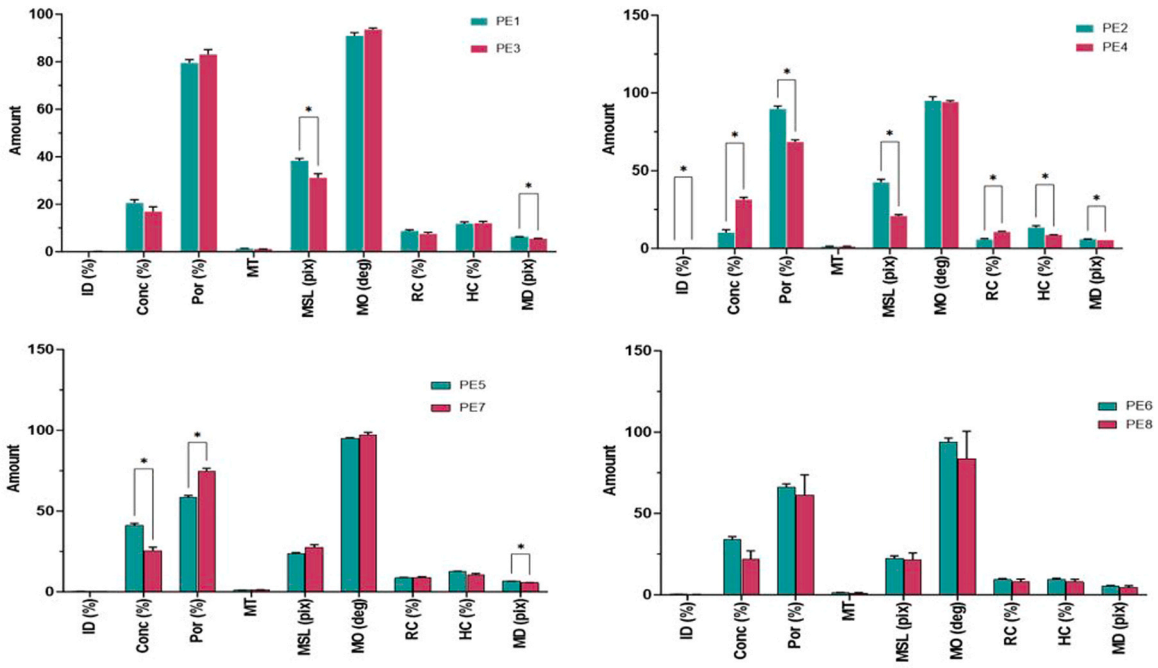

Fig. 6. Effect of levonorgestrel (LNG) on morphological properties of electrospun fibers. **ID = Intersection Density, Conc = Concentration, Por = Porosity, MT= Mean Tortuosity, MSL= Mean Segment Length, MO= Mean Orientation, RC= Radial Count, HC= Horizontal Count MD = Mean Diameter.**

finding is consistent with observations by Dehghan *et al.* [41], who reported that the addition of nanoparticles to electrospun fibers affected fiber diameter and mat porosity. While they focused on different materials, the principle that additives can influence fiber mat structure appears to hold true in both cases. In essence, the concentration of fiber could be an important factor in determining the overall properties of electrospun nanofiber mats. Higher concentrations might lead to stronger inter-fiber bonding, potentially affecting mechanical strength, porosity, and drug release characteristics in drug-loaded fibers.

3.1.3. *Porosity of electrospun fibers (%)*

From Fig. 3D, there was observed significant difference in the porosity among the formulations with the highest being PE2 (89.76 ± 5.63 %). Further, the addition of CAP/HA significantly affected the porosity of the fibers. PE5, which included the surfactant and HA, had a significantly lower porosity compared to PE1, which did not include the surfactant ($p < 0.001$). Similarly, PE6, which also had the surfactant and HA, exhibited a significantly lower porosity than PE2 ($p < 0.001$). For PE7, the inclusion of the surfactant and HA resulted in a porosity significantly lower than that of PE2 ($p < 0.001$) but was not significantly different from PE3 ($p > 0.05$). Finally, PE8 demonstrated a significantly lower porosity compared to PE2 ($p < 0.001$) and PE3 ($p = 0.03$). The plate collector type used in PE2 significantly increased the porosity of the fiber (89.76 %) compared to PE1 (79.49 %) ($p = 0.000540$), and PE4 (68.48) showed a significantly lower Porosity compared to PE3 (83.11 %) ($p = 0.000030$) (Fig. 5). Porosity was significantly decreased in PE4 (68.48 %) compared to PE2 (89.76 %) ($p < 0.001$) upon the presence of 1.96 % LNG and increased it significantly in PE7 (74.45 %) compared to PE5 (58.67 %) ($p = 0.0005$) (Fig. 6).

The porosity results demonstrated an inverse relationship with concentration of fibers, which is logically consistent given that higher fiber concentration would likely lead to reduced void space. PE5 had the lowest porosity (58.67 %), while PE2 had the highest (89.76 %). The porosity values observed in this study vary significantly across different formulations. These broad range of porosity values extends beyond what might be inferred from Rambabu *et al.* [39], who reported that approximately 67 % of their prepared nanocellulose fibers exhibited a diameter range between 5 and 25 nm. In general, there is an inverse relationship between fiber diameter and porosity—thinner fibers tend to form denser, less porous mats, while thicker fibers create more open, porous structures. The current study's findings suggest that formulation and processing parameters can produce a wider range of porosities, which could be valuable for various applications. The effect of collector type on porosity (PE2: 89.76 % vs PE1: 79.49 %) and the influence of LNG (PE4: 68.48 % vs PE2: 89.76 %) point out that both collector type and additives can be used to fine-tune porosity, which could be particularly relevant for applications such as drug release and filtration. This is parallel with the general approach of Dehghan *et al.* [41], who optimized various parameters for air filtration applications, although they didn't specifically report on the effects of collector type or LNG on porosity.

3.1.4. *Tortuosity of electrospun fibers,*

From the results in (Fig. 3G), there was no significant difference in the mean tortuosity (MT) across all samples. Across all comparisons, the addition of the surfactant did not lead tosignificant changes in the tortuosity of the fibers (all $p > 0.05$). Based on the collector types, there were no significant differences in mean tortuosity between PE2 (1.35) and PE1 (1.32) ($p = 0.83$), between PE4 (1.35) and PE3 (1.12) ($p = 0.10$), between PE6 (1.36) and PE5 (1.09) ($p = 0.08$), and between PE8 (1.37) and PE7 (1.16) ($p = 0.26$). No significant differences in MT were observed with the addition of LNG between the fibers.

When compared to the results of Amiraliyan *et al.* [40], who reported that solution concentration had a significant effect on fiber diameter and its standard deviation, there was no observed significant effect. While fiber diameter and tortuosity are different properties, it is expected that factors affecting fiber formation would also influence tortuosity [42]. The lack of significant differences in tortuosity suggests that this property may be less sensitive to formulation and processing parameters than other fiber characteristics. The consistent tortuosity across different conditions points out that the basic fiber formation process during electrospinning may be highly reliable and not easily affected by variations in collector type, drug incorporation, or surface treatments meanwhile in other studies, the release rate of encapsulated drugs or the permeability of the scaffold was observed to be influenced by tortuosity [43–45]. However, it has been found that the variables tested in this

study do not have a significant impact on tortuosity. This suggests that other factors, such as fiber diameter or porosity, may be more important in controlling these properties.

3.1.5. Mean segment length

In the analysis of the mean segment length (MSL) of the fibers from Fig. 3C, PE2 (42.55 ± 5.84 pix) had the highest observed MSL. The addition of the surfactant generally resulted in shorter fiber lengths. The MSL decreased significantly from 38.33 ± 3.03 pix in PE1 to 23.70 ± 1.36 in PE5 ($p < 0.001$) (Fig. 4). The MSL also decreased significantly from 42.55 ± 5.84 pix in PE2 to 22.40 ± 3.63 in PE6 ($p < 0.001$), and from 31.15 ± 5.31 in PE3 to 27.66 ± 3.52 in PE7 ($p > 0.05$), showing a trend towards shorter fibers with the addition of the surfactant. Also, there was a slight increase in MSL from 20.94 ± 2.13 in PE4 to 25.58 ± 3.18 in PE8 ($p > 0.05$). The effect of the collector types on the fibers showed no significant differences in MSL between PE2 and PE1 ($p = 0.08$). However, the MSL was significantly shorter in PE4 (wire collector) compared to PE3 (plate collector) ($p = 0.000116$). In addition, there was a reduced MSL in PE4 compared to PE2 ($p < 0.000001$), and in PE3 compared to PE1($p = 0.002221$) upon the addition of LNG (Fig. 6)

The study observed significant variations in mean segment length (MSL) across different formulations, with the addition of surfactant generally resulting in shorter fiber lengths. For instance, MSL decreased significantly from 38.33 ± 3.03 pix in PE1 to 23.70 ± 1.36 pix in PE5 ($p < 0.001$). This finding echoes the observations of Gu, Ren, and Vancso [46], who reported that solution properties significantly affected fiber morphology. The consistent reduction in MSL observed in different samples when surfactant, HA coating, and LNG was added indicates that these treatments have an observed effect on fiber morphology. This is essential for applications that require consistent results and precise control over the material's microstructure. The results show that these variables can be strategically adjusted to regulate the length of the fiber segments, which ultimately affects the overall structure and potential uses of the scaffold [47,48]. Through incorporating surfactant and LNG, especially when utilizing a wire collector, it becomes clear that there is potential for generating more compact and consistent fiber networks. This could prove beneficial in drug delivery and biomedical applications.

3.1.6. Mean fiber orientation

In the analysis of the mean orientation (MO) expressed in deg of the fibers from Fig. 3E, PE8 (100.48 ± 4.65) had the highest MO. The addition of the surfactant resulted in a slight increase in mean orientation from 90.98 ± 4.11 in PE1 to 94.99 ± 0.90 in PE5 ($p > 0.05$). MO also changed marginally from 95.01 ± 7.72 in PE2 to 94.02 ± 5.77 in PE6 with the addition of surfactant. Again, this difference was not statistically significant ($p > 0.05$). When LNG was present in the plate collector setup, the addition of the surfactant led to a slight increase in mean orientation from 93.58 ± 2.06 in PE3 to 97.06 ± 3.65 in PE7 ($p > 0.05$). Further, MO increased from 94.21 ± 2.34 in PE4 to 100.48 ± 4.65 in PE8. While this increase was more substantial compared to other conditions, it was only statistically significant when compared to PE1 ($p < 0.01$), but not when compared to PE4 or any other experimental conditions ($p > 0.05$). The collector types had no significant effect on the mean orientation between PE2 and PE1, ($p = 0.187733$), between PE4 and PE3 ($p = 0.572628$), between PE6 and PE5 ($p = 0.70$), and between PE8 (100.5) and PE7 (97.06) ($p = 0.23$). No significant differences in orientation were observed with the addition of LNG between the fibers.

The study found minimal significant differences in fiber orientation across formulations, with only PE8 showing a significant difference from PE1 ($p < 0.01$). This relative consistency in orientation contrasts with the findings of Zhang *et al.* [49], who reported that take-up velocity significantly affected fiber orientation. Zhang *et al.* observed "remarkable crystalline and amorphous orientation" in fibers prepared from high molecular weight polymers at high take-up velocities. The collector type was found to have no impact on the orientation and could be because both plate and wire collectors are capable of producing relatively uniform electric fields during electrospinning, leading to consistent fiber deposition regardless of the collector type. Additionally, the overall experimental conditions (such as voltage, flow rate, and distance) might have been optimized to minimize variations in fiber orientation. Drug incorporation was seen not to disrupt structural integrity as the molecular structure and distribution of LNG within the polymer matrix might not interfere with the forces driving fiber alignment during electrospinning. Additionally, the concentration of LNG may be low enough not to significantly impact the rheological properties of the electrospinning solution, which could affect fiber orientation. Surfactants like CAP can reduce the surface tension of the electrospinning solution, potentially leading to more uniform fiber formation and slight improvements in alignment. However, in this study, the changes were not large enough to produce significant differences, possibly because the overall fiber formation process remained dominated by the electrospinning parameters and collector geometry. Hence the formulation and processing parameters investigated may have less impact on fiber orientation than the take-up velocity. These findings have a positive impact on LNG delivery. The consistent fiber orientation across different conditions points out that the nanofibers will provide uniform and predictable drug release profiles and maintain mechanical stability.

3.1.7. Diameter of electrospun fibers

The mean diameter (MD) from Fig. 3E showed that PE5 (6.61 ± 0.06 pix) had the highest observed MD. In the plate collector setup without LNG, the addition of the surfactant resulted in an increase in mean fiber diameter from 6.28 ± 0.27 pix in PE1 to 6.61 ± 0.06 pix in PE5. Although this increase was observed, it was not statistically significant ($p > 0.05$). Addition of CAP led to a decrease in mean fiber diameter from 5.99 ± 0.27 pix in PE2 to 5.61 ± 0.10 pix in PE6 ($p = 0.02$), the surfactant also resulted in a slight increase in mean fiber diameter from PE3 to PE7 ($p > 0.05$), and a marginal increase in mean fiber diameter from PE4 to PE8 ($p > 0.05$). PE5 showed significant differences from PE2, PE3, and PE4 ($p < 0.001$ for all comparisons), and PE6, PE7, and PE8 (all with surfactant) showed significant differences from PE1 (without surfactant) ($p < 0.001$ for all comparisons). Concerning the effects of the collector types used, the results did not reveal any significant differences in MD between PE2 and PE1 ($p = 0.03$). MD was significantly lower in PE6 compared to PE5 ($p < 0.000001$), and in PE8 (5.61 pix) compared to PE7 (5.65 pix) ($p = 0.782091$) (Figure 1.2). The results showed that there was a decreased MD in PE3 (5.56 pix) compared to PE1 (6.28 pix) ($p = 0.000003$) with the addition of LNG, in PE4 (5.38 pix) compared to PE2 (5.99 pix) ($p = 0.000081$), and in PE7 (5.65 pix) compared to PE5 (6.61 pix) ($p = 0.0014$).

The findings suggests that the addition of surfactant and LNG generally led to decreased fiber diameters; For instance, the mean diameter decreased from 6.28 ± 0.27 pix in PE1 to 5.56 ± 0.20 pix in PE3 ($p < 0.001$) with the addition of LNG and are consistent with the observations of Doustgani [50], who reported that solution concentration significantly affected nanofiber diameter. The addition of LNG causing a decrease in fiber diameter is indicative that the drug may be impacting the electrospinning process. This could be due to its effects on the viscosity or surface tension of the polymer solution. Thinner fibers could potentially increase the surface area-to-volume ratios, resulting in a potential improvement in the rate of drug release from the fibers [9]. This could be advantageous for applications where immediate drug release of the drug is preferred. The difference in MD between collector types might be attributed to variations in electric field distribution during electrospinning. Wire collectors often create more focused and intense electric fields, leading to more stretching and thinner fibers. The general trend in the study shows that both the addition of LNG and the use of a surfactant tend to reduce the MD of the fibers. This suggests that these components influence the fiber formation process, possibly by

affecting the physical properties of the electrospinning solution. The reduced MD could have several implications for the scaffold's performance, particularly in drug delivery, where thinner fibers with smaller diameters might enhance drug release kinetics.

3.2. Mechanical properties of electrospun nanofibers

3.2.1. Tensile strength

The tensile strength of electrospun fibers is seen in (Fig. 7A). PE1, which used a plate collector without LNG, exhibited an ultimate tensile strength (UTS) of 0.07 ± 0.03 MPa. In comparison, PE2 had a UTS of 0.07 ± 0.04 MPa. The tensile strength values of these two samples were quite similar, indicating that the type of collector (plate vs. wire) had a minimal effect on the tensile strength of the fibers in the absence of LNG. When 1.96 % w/w LNG was incorporated, the tensile strength values showed a notable difference between the collector types. For the samples incorporating both LNG and the additional treatments of CAP and HA coating, PE7 had a UTS of 0.08 ± 0.05 MPa, and PE8 showed a UTS of 0.06 ± 0.01 MPa. Similar to the trend observed in PE3 and PE4, PE7 demonstrated a higher tensile strength compared to PE8, though the difference was not as pronounced as in the case without the additional treatments. From the results obtained from the study, it was observed that the incorporation of LNG decreased the ultimate tensile strength (UTS) for all comparisons. This finding agrees with the observations of Conte *et al.* [36], who reported that fiber density correlates with mechanical properties. They found that ultimate tensile strength increased with increasing fiber density, from 594 MPa for samples electrospun for 30 seconds to 1250 MPa for samples electrospun for 40 minutes.

The addition of CAP as a surfactant and an outer coating of HA slightly increased the tensile strength in our study. This is in line with the findings of Amiri *et al.* [51], who reported that chitosan-gelatin blend nanofibers had higher Young's moduli than chitosan nanofibers alone, and these values increased significantly after cross-linking. Also, Zhang *et al.* [49] observed that the molecular weight of poly(l-lactide) (PLLA) and take-up velocity during electrospinning affected the tensile strength of the resulting fibers. They found an optimum processing condition for achieving mechanically superior PLLA fibers, which supports our observation that preparation methods significantly influence mechanical properties.

3.2.2. Young's modulus

The Young's modulus values of the nanofiber samples showed variations based on their preparation methods (Fig. 7B). PE1, using a plate collector without LNG, exhibited a Young's modulus of 5.02 ± 4.40 MPa, indicating moderate stiffness. In contrast, PE2, using a wire collector without LNG, showed a substantially higher Young's modulus of 23.02 ± 20.74 MPa. The incorporation of LNG further increased the Young's modulus in PE3 to 28.66 ± 20.29 MPa, highlighting a significant enhancement in fiber stiffness with LNG. However, PE4 had a lower Young's modulus of 9.01 ± 6.05 MPa compared to PE3, indicating a more variable effect of LNG depending on the collector type. For samples PE5 to PE8, which included an outer coating of HA and the use of CAP as a surfactant, the Young's modulus values generally decreased compared to their non-coated counterparts. PE5, corresponding to PE1's conditions but with additional treatments, showed a significantly lower Young's modulus of 1.54 ± 0.81 MPa, and PE6, similar to PE2 but with additional treatments, also had a reduced Young's modulus of 2.17 ± 1.97 MPa. PE7 and PE8, corresponding to PE3 and PE4 respectively but with the extra coatings, exhibited Young's modulus values of 2.54 ± 1.28 MPa and 5.38 ± 4.22 MPa.

According to the findings of this study, the wire collector without LNG (PE2) showed a substantially higher Young's modulus (23.02 ± 20.74 MPa) compared to the plate collector without LNG (PE1, 5.02 ± 4.40 MPa). This finding contrasts with the results of Conte *et al.* [26], who observed that Young's modulus decreased as fiber density increased, from 14,901 MPa for samples electrospun for 30 seconds to 3615 MPa for samples electrospun for 40 minutes. The incorporation of the active, LNG further increased the Young's modulus in the plate collector sample (PE3) from 5.022 ± 4.40 MPa to 28.66 ± 20.29 MPa. However, the effect was not consistent across collector types suggesting LNG significantly impacts the influence of collector type on the young modulus of the fibers. This variability in results emphasizes the relationship between multiple factors affecting nanofiber mechanical properties, each exerting more influence than the other as noted by Gu, Ren, and Vancso [46], in their study of polyacrylonitrile (PAN) nanofibers. The low tensile strength may be attributed to the presence of HA, which contains amide and carboxylate groups with negative charges that can form hydrogen bonds to attract water molecules. These water molecules can break the hydrogen bonds within the molecular chains of the electrospun scaffold, leading to a decrease in its tensile strength [52].

3.2.3. Elongation at break

The elongation at break percentage of the nanofiber samples, which measures the extent to which fibers can stretch before breaking showed variations (Fig. 7C). PE1, using a plate collector without LNG, had an elongation at break of 39.09 ± 4.82 %, indicating a high degree of flexibility. PE2, using a wire collector without LNG, showed a lower elongation at break of 28.06 ± 8.35 %. The addition of LNG in PE3 further increased the elongation at break to 45.27 ± 2.92 %. However, PE4 had a lower elongation at break of 30.94 ± 1.37 % and samples PE5 to PE8, which included an outer coating of HA and the use of CAP as a surfactant, had elongation at break values that generally decreased compared to their non-coated counterparts. PE5, which matched PE1's conditions but with additional treatments, exhibited a much lower elongation at break of 8.17 ± 2.17 %, and PE6, similar to PE2 but with

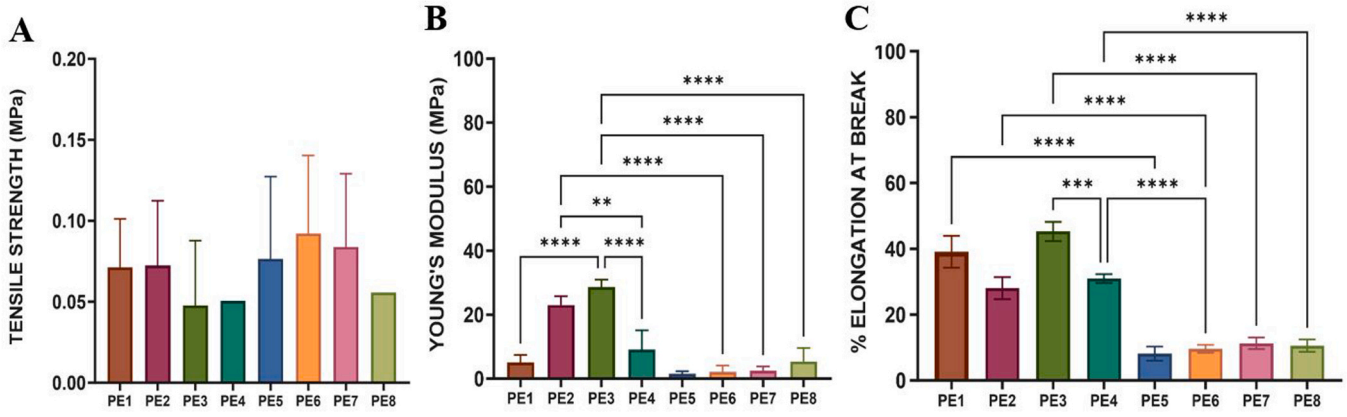

Fig. 7. (A)Tensile Strength (B) Young's modulus (C) Elongation at break (%) of the electrospun fibers.

additional treatments, showed an elongation at break of 9.61 ± 1.20 %. PE7 and PE8, corresponding to PE3 and PE4 respectively but with the extra coatings, exhibited elongation at break values of 11.27 ± 1.77 % and 10.61 ± 1.87 %.

This study found that the elongation at break percentage varied significantly among the samples, with the plate collector without LNG (PE1) showing a high degree of flexibility (39.09 ± 4.82 %). The addition of LNG further increased it to 45.27 ± 2.92 % in PE3. These findings are in line with the observations of Conte *et al.* [36], who reported that the ultimate tensile strain increased from 0.39 for samples electrospun for 30 seconds to 0.48 for samples electrospun for 40 minutes. However, the addition of HA coating and CAP surfactant significantly reduced the elongation at break in our study. This highlights the importance of considering the effects of additives on mechanical properties, a point also emphasized by Stachewicz *et al.* [38] in their study of polyamide 6 (PA6) nanofiber composites with polyvinyl alcohol (PVA) matrix.

The variability in mechanical properties observed across these studies underscores the complexity of nanofiber production and the need for careful optimization of preparation methods. As noted by Doustgani [50], in the study of poly(vinyl alcohol) (PVA) nanofibers, solution concentration was found to be the most significant parameter affecting nanofiber diameter, which in turn influences mechanical properties. The trade-offs between different mechanical properties observed in our study are consistent with findings from other researchers. For example, Rambabu *et al.* [39] reported that optimizing the pretreatment and mechanical grinding of cellulosic fibers led to nanofibers with both high tensile strength (273 MPa) and modulus (17 GPa), demonstrating the potential for achieving balanced mechanical properties through careful process control. These findings collectively suggest that the optimal preparation method for electrospun nanofibers depends on the specific application requirements. For instance, if high tensile strength is crucial, our study suggests a plate collector with LNG might be preferred, while Zhang *et al.* [49], indicated that optimizing the molecular weight and take-up velocity of PLLA fibers could achieve similar results. The importance of process parameters in determining nanofiber properties is further emphasized in studies that used response surface methodology to establish quantitative relationships between electrospinning parameters and fiber characteristics [50, 53,54].

3.3. Encapsulation efficiency, drug loading and fiber yield of electrospun nanofibers

The encapsulation efficiency, drug loading and fiber yield of the nanofibers were calculated as illustrated in Fig. 8A, B and C. PE3 (plate collector) exhibited a superior drug loading of 3.62 ± 0.02 %, although demonstrated a diminished encapsulation efficiency of 28.15 ± 0.05 % and a fiber yield of 16.28 %; conversely, PE4 (wire collector) revealed a lesser drug loading of 3.56 ± 0.05 %, accompanied by an enhanced encapsulation efficiency of 37.50 ± 0.01 % and a fiber yield of 22.09 %. On addition of a surfactant and coating with HA, the wire collector (PE8) was observed to possess higher drug loading 5.7 ± 0.01 % compared to PE7 (Plate collector) 5.1 ± 0.02 %, ** **$p < = 0.001$. The wire collectors consistently had a higher encapsulation efficiency (PE4, 20.81 ± 0.1 % and PE8, 37.5 ± 0.05 %) and fiber yield (PE4, 22.09 ± 0.5 % and PE8 33.81 ± 0.5 %) for each comparison groups. Fibers PE7 and PE8 consistently had higher values compared to PE3 and PE4. In a study conducted with PCL, fibers were obtained utilizing three distinct types of collectors: a spinning drum, static copper wires, and a rotating mandrel. When a revolving drum was employed, fibers were elongated by the force of rotational velocity, aligning and diminishing fiber widths. The utilization of a static collector caused electrostatic forces to stretch fibers transversely across the wires, producing densely aligned fibers perpendicular to the wires. Conversely, when a rotating mandrel was utilized,

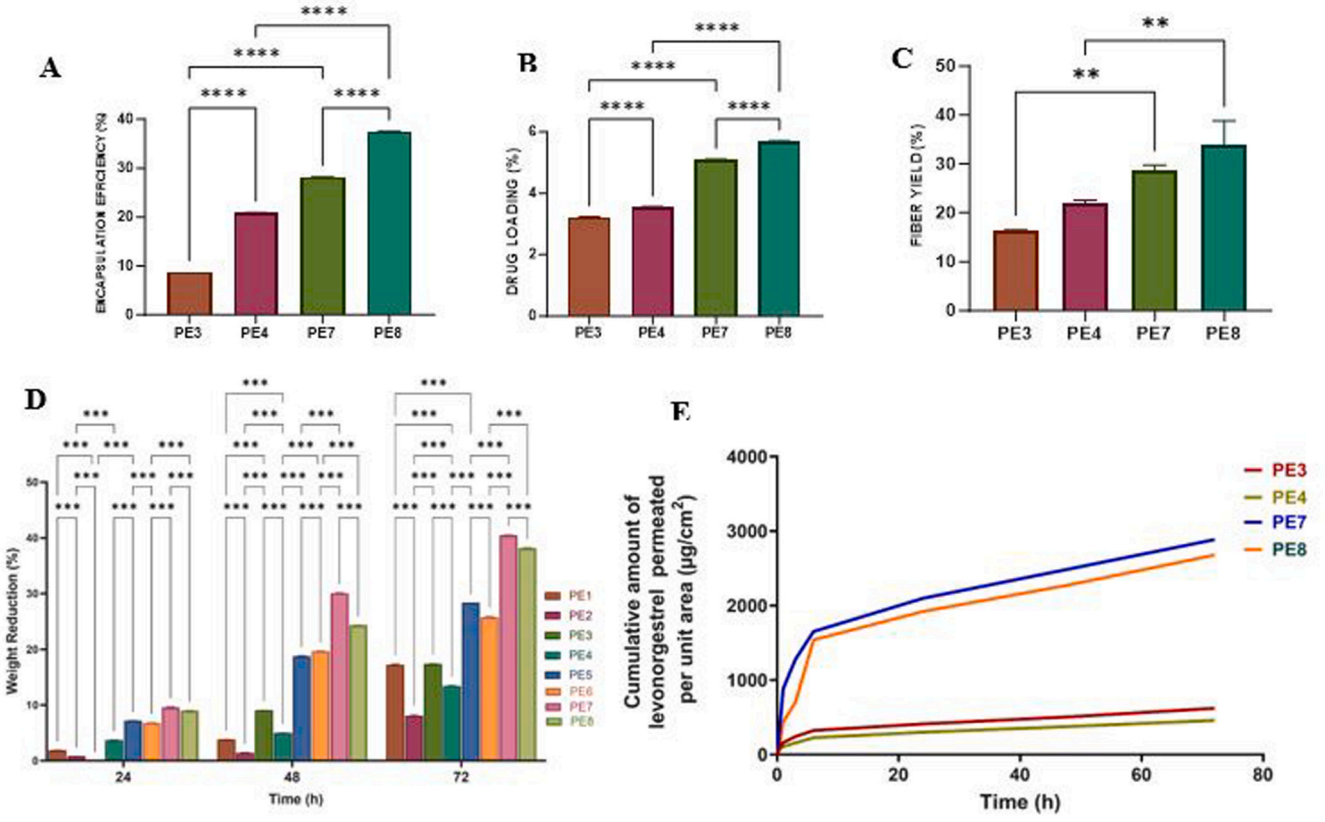

Fig. 8. A) Encapsulation efficiency B) Drug loading C) Fiber yield D) % weight reduction of electrospun scaffolds in SVF/SF E) Release profiles of LNG in PE3, PE4, PE7 and PE8 electrospun scaffolds containing LNG in SVF/SF. *$P < =0.05$, * *$p < = 0.01$, * **$p < = 0.001$, * ** *$p < = 0.0001$).

electrostatic forces drew fibers parallel to the axis, resulting in the formation of fused fibers transversely to the axis at elevated rotational speeds [55]. If the collector type changes fiber morphology and alignment in this manner, there is an influence on drug loading, encapsulation efficiency and fiber yield. In a study on LNG, the observed drug loading was 9.5 %, 15.9 %, and 22.2 %, while the encapsulation efficiency (EE) was 1.2 % and 2.3 %, compared to the theoretical drug loading of 10.0 %, 17.0 %, and 23.0 % for Gelatin/LNG fibers, respectively. The findings indicated a drug loading of over 90 % for all formulations. The encapsulation efficiency (EE%) ranged from 90 % to 110 % for all fiber types and this high efficiency was linked to the extensive surface area of the fibers. Furthermore, the passive drug loading approach, shown by electrospinning, entails the integration of the drug into the polymeric solution prior to spinning and solidification, hence reducing the likelihood of drug loss during the process [56].

3.4. Biodegration of electrospun nanofibers

Biodegradation was observed using the % weight reduction of the electrospun nanofibers (Fig. 8D) and the degradation was time-based with the highest rates occurring in 72 h for all comparison groups. The wire collector was observed to have a higher % weight reduction $p \leq 0.01$ for all comparison groups. After 24 hours, most formulations showed minimal change; PE7 and PE8 showed substantially larger weight declines 9.6 ± 0.1 % and 9.0 ± 0.01 % respectively, while PE3 and PE4 revealed the least degradation 0.00 % and 3.68 ± 0.04 % respectively. The rates of degradation revealed more obvious variations after 48 hours. PE7 dropped over half of its weight after 72 hours followed by PE8.

The reported degradation rate might have been impacted by the collector type, polymer mix, and LNG. Combining PLGA with PCL enhances biodegradation of PCL, nevertheless enabling it to hydrolyze with time; PLGA is well-known for its biodegradability. The choice of collector (plate or wire) was seen to alter the scaffold geometry and porosity, therefore influencing the exposure of the nanofibers to the SVF/SF and, hence, the degradation rate. Electrospraying the PE5-PE7 group with hyaluronic acid (HA) in the formulations was observed to increase the hydrophilicity of the nanofibers hence the observed degradation rate which was higher than the other group PE1-PE4, therefore encouraging water absorption and later polymer chain hydrolysis. HA has limited stability in the body due to its fast breakdown by hyaluronidase and reactive oxygen species, which results in its degradation [57]. PE1-PE4 showed more robust polymer networks either from higher cross-linking densities or stronger intermolecular pressures, which reduced their sensitivity to breakdown. From the mechanical properties, the fibers had a higher elongation at break, and this could be responsible for the decreased degradation. These formulations can hence be employed for delivery of sustained release LNG.

3.5. In vitro drug release of LNG in SVF/SF

Fig. 8E illustrates the cumulative amount of LNG permeated per unit area for PE3, PE4, PE7 and PE8 in SVF/SF. Human vaginal fluid averages 6 g daily, with 0.5–0.75 g in the vagina at any one instance [58]. The daily LNG release corresponds to the drug's matrix type kinetics. The permeated doses were observed to range from 87.12 to 115.70 μg/cm^2 for PE3, and 74.09–82.26 μg/cm^2 for PE4 daily. For PE7 and PE8, 355.321–402.313 μg/cm^2 and 392.243–397.518 μg/cm^2 was observed daily. The daily permeated dosage for LNG obtained from gelatin nanofibers using a transdermal patch designed for *in vitro* release was around 120–170 μg/cm^2 [53]. For PE3, 66.19 % of drug was released in 24 h, for PE4, 65.48 % was released. PE7 72.64 % and PE8 71.72 %. There was an observed direct relationship between the degradation of the electrospun nanofibers and its drug release. The release of levonorgestrel from the polymeric systems was strongly influenced by the rate of polymer biodegradability. Rapidly biodegradable polymer systems like PE7 and PE8 showed significant cumulative drug release with an initial burst impact, thereby reaching > 3000 μg/cm^2 by 72 hours. Faster drug diffusion was made possible by the generation of holes and microchannels in the polymer matrix as it degrades, hence releasing bursts. By contrast, PE3 and PE4 degraded down more slowly, generating somewhat modest drug release rates below 1500 μg/cm^2. Their linear and steady release patterns point todiffusion. Although fast-degrading polymers are suitable for immediate-release formulations when a rapid therapeutic effect is required, slower-degrading polymers are better suited for sustained-release systems as they provide controlled, long-term drug delivery. This is important for LNG targeted release.

4. Limitations of the study

With the ever-increasing research carried out on nanofibers, little attention has been paid to in-depth analysis of microstructural architecture of these nanofibers. Increasing attention is given to nanofiber diameter and porosity and performance with regards degradation and release but less on other parameters such as intersection density, concentration of fibers, fiber orientation etc. These parameters are seen to impact on mechanical properties, drug loading, degradation and drug release hence this has lessened availability of studies for comparative purposes, hampering benchmarking and evaluation of current findings.

5. Conclusion

This study on electrospun fibers composed of PCL, PLGA, and HA loaded with LNG has highlighted the relationships between formulation parameters and processing parameters, on the resulting fiber characteristics. The investigation demonstrated that collector type, surfactant inclusion, and processing conditions significantly influenced both microstructural architecture and mechanical properties of the electrospun nanofibers. The findings include the combined influence of LNG and collector type on fiber diameter and tensile strength, the relationship between concentration and mechanical properties, and the impact of surfactants and coatings on fiber length and overall performance. The image-analysis technology offered a significant benefit by allowing the measurement and analysis of many micro-architectural properties. It was observed that fiber tortuosity can be utilized to optimize the parameters of a probability density function that characterizes the gradual involvement of fibers in relation to strain. Intersections can have an impact on the stiffness and concentrations of fibers, which in turn can affect fiber properties. These, integrated with the fiber diameter distribution can be utilized to characterize the section properties of each finite element, to depict the fiber skeleton network. Optimizing these properties will influence Levonorgestrel loading into fiber mat to deliver low dose LNG combating dose dependent side effects. Future study should prioritize understanding the effect of these characteristics on drug loading and drug release and enhancement of the microstructural and mechanical properties of PCL/PLGA/HA-loaded LNG nanofibers to such that fits the delivery of low dose LNG for contraception.

CRediT authorship contribution statement

Conceptualization: Margaret O. Ilomuanya, Peace-OfonAbasi O. Bassey, Alkiviadis Tsamis. **Methodology and Validation:** Margaret O. Ilomuanya, Peace-OfonAbasi O. Bassey, Dimitrios Tsamos, Alkiviadis Tsamis, Alexandros E. Tsouknidas. **Formal analysis and Investigation:** Peace-OfonAbasi O. Bassey, Alkiviadis Tsamis, Bukola A. Oseni, Deborah A. Ogundemuren, Karamot O. Oyediran, Evans N. Ekeji, Bryan C. Okubwa. **Resources:** Margaret O. Ilomuanya. **Data Curation:** Dimitrios Tsamos, Alkiviadis Tsamis, Alexandros E. Tsouknidas, David Vorp. **Writing — original draft:** Peace-OfonAbasi O. Bassey. **Writing — final draft:** Peace-OfonAbasi O. Bassey, Bukola A. Oseni, Evans N. Ekeji, Bryan C. Okubwa. **Visualization:** Peace-OfonAbasi O. Bassey,

Alkiviadis Tsamis, Deborah A. Ogundemuren, Karamot O. Oyediran, Evans N. Ekeji, Bryan C. Okubwa. **Supervision:** Margaret O. Ilomuanya, Samson O. Adeosun. **Project administration:** Margaret O. Ilomuanya, Alkiviadis Tsamis. **Funding acquisition:** Margaret O. Ilomuanya. All authors have reviewed and consented to the final version of the manuscript that has been published.

Declaration of Competing Interest

The authors declare that they have no known competing financial interests or personal relationships that could have appeared to influence the work reported in this paper.

Acknowledgment

This research was funded by MEDAFRICA Foundation Inc. Scotch Plains, NJ, USA award number 01/2021/22.

Data Availability

Data will be made available on request.

References

[1] A. Ghajarieh, S. Habibi, A. Talebian, Biomedical applications of nanofibers, Russ. J. Appl. Chem. 94 (2021) 847–872, https://doi.org/10.1134/S1070427221070016.
[2] S. Sabra, D.M. Ragab, M.M. Agwa, S. Rohani, Recent advances in electrospun nanofibers for some biomedical applications, Eur. J. Pharm. Sci. 144 (2020) 105224, https://doi.org/10.1016/j.ejps.2020.105224.
[3] M.K. Gaydhane, C.S. Sharma, S. Majumdar, Electrospun nanofibres in drug delivery: advances in controlled release strategies, RSC Adv. 13 (2023) 7312–7328, https://doi.org/10.1039/D2RA06023J.
[4] B. Singh, K. Kim, M.-H. Park, On-demand drug delivery systems using nanofibers, Nanomaterials 11 (2021) 3411, https://doi.org/10.3390/nano11123411.
[5] A. Nadaf, A. Gupta, N. Hasan, N. Fauziya, S. Ahmad, P. Kesharwani, et al., Recent update on electrospinning and electrospun nanofibers: current trends and their applications, RSC Adv. 12 (2022) 23808–23828, https://doi.org/10.1039/d2ra02864f.
[6] Y.J. Son, W.J. Kim, H.S. Yoo, Therapeutic applications of electrospun nanofibers for drug delivery systems, Arch. Pharm. Res 37 (2014) 69–78, https://doi.org/10.1007/s12272-013-0284-2.
[7] J.N. Amajuoyi, M.O. Ilomuanya, Y. Asantewaa-Osei, C.P. Azubuike, S.O. Adeosun, C.I. Igwilo, Development of electrospun keratin/coenzyme Q10/poly vinyl alcohol nanofibrous scaffold containing mupirocin as potential dressing for infected wounds, Futur J. Pharm. Sci. 6 (2020), https://doi.org/10.1186/s43094-020-00043-z.
[8] M.O. Ilomuanya, B.A. Oseni, B.C. Okwuba, P. Abia, M.I. Aboh, O.P. Oluwale, et al., International Journal of Biological Macromolecules Evaluation of MDR-specific phage P ϕ -Mi-Pa loaded mucoadhesive electrospun nanofibrous scaffolds against drug-resistant Pseudomonas aeruginosa - induced wound infections in an animal model, Int J. Biol. Macromol. 277 (2024) 134484, https://doi.org/10.1016/j.ijbiomac.2024.134484.
[9] M.O. Ilomuanya, P.O. Bassey, D.A. Ogundemuren, U.N. Ubani-ukoma, A. Tsamis, Y. Fan, et al., Development of mucoadhesive electrospun scaffolds for intravaginal delivery of Lactobacilli spp., a tenside, and metronidazole for the management of bacterial vaginosis 2023, Pharmaceutics 15 (2023) 1263, https://doi.org/10.3390/pharmaceutics15041263.
[10] E. Archer, M. Torretti, S. Madbouly, Biodegradable polycaprolactone (PCL) based polymer and composites, Phys. Sci. Rev. 8 (2023) 4391–4414, https://doi.org/10.1515/psr-2020-0074.
[11] J.R. Dias, A. Sousa, A. Augusto, P.J. Bártolo, P.L. Granja, Electrospun polycaprolactone (PCL) degradation: an in vitro and in vivo study, Polymers 14 (2022) 1–15, https://doi.org/10.3390/polym14163397.
[12] Y.R. Chavan, S.M. Tambe, D.D. Jain, S.V. Khairnar, P.D. Amin, Redefining the importance of polylactide-co-glycolide acid (PLGA) in drug delivery, Ann. Pharm. Françaises 80 (2022) 603–616, https://doi.org/10.1016/j.pharma.2021.11.009.
[13] E. Lagreca, V. Onesto, C. Di Natale, S. La Manna, P.A. Netti, R. Vecchione, Recent advances in the formulation of PLGA microparticles for controlled drug delivery, Prog. Biomater. 9 (2020) 153–174, https://doi.org/10.1007/s40204-020-00139-y.
[14] A. Sionkowska, M. Gadomska, K. Musiał, J. Piątek, Hyaluronic acid as a component of natural polymer blends for biomedical applications: a review, Molecules 25 (2020) 4035, https://doi.org/10.3390/molecules25184035.
[15] G. Abatangelo, V. Vindigni, G. Avruscio, L. Pandis, P. Brun, Hyaluronic acid: Redefining its role, Cells 9 (2020) 1–19, https://doi.org/10.3390/cells9071743.
[16] F. Gisbert Roca, P. Lozano Picazo, J. Pérez-Rigueiro, G.V. Guinea Tortuero, M. Monleón Pradas, C. Martínez-Ramos, Conduits based on the combination of hyaluronic acid and silk fibroin: Characterization, in vitro studies and in vivo biocompatibility, Int J. Biol. Macromol. 148 (2020) 378–390, https://doi.org/10.1016/j.ijbiomac.2020.01.149.
[17] G. Agarwal, S. Agiwal, A. Srivastava, Hyaluronic acid containing scaffolds ameliorate stem cell function for tissue repair and regeneration, Int J. Biol. Macromol. 165 (2020) 388–401, https://doi.org/10.1016/j.ijbiomac.2020.09.107.
[18] P. Zhai, X. Peng, B. Li, Y. Liu, H. Sun, X. Li, The application of hyaluronic acid in bone regeneration, Int J. Biol. Macromol. 151 (2020) 1224–1239, https://doi.org/10.1016/j.ijbiomac.2019.10.169.
[19] S. Jin, X. Xia, J. Huang, C. Yuan, Y. Zuo, Y. Li, et al., Recent advances in PLGA-based biomaterials for bone tissue regeneration, Acta Biomater. 127 (2021) 56–79, https://doi.org/10.1016/j.actbio.2021.03.067.
[20] T. Tang, T. Shi, D. Li, J. Xia, Q. Hu, Y. Cao, Adsorption properties and degradation dynamics of endocrine-disrupting chemical levonorgestrel in soils, J. Agric. Food Chem. 60 (2012) 3999–4004, https://doi.org/10.1021/jf300479z.
[21] L.M. Lopez, D.A. Grimes, M.F. Gallo, L.L. Stockton, K.F. Schulz, Skin patch and vaginal ring versus combined oral, Ovid Medlin Database Syst. Rev. (2013), https://doi.org/10.1002/14651858.CD003552.pub4.www.cochranelibrary.com.
[22] M. Shohel, M.M. Rahman, A. Zaman, M.M.N. Uddin, M.M. Al-Amin, H.M. Reza, A systematic review of effectiveness and safety of different regimens of levonorgestrel oral tablets for emergency contraception, BMC Women's. Health 14 (2014) 54, https://doi.org/10.1186/1472-6874-14-54.
[23] Y. Kitani, T. Ishiguro, A. Kobayashi, R. Tamura, H. Ueda, S. Adachi, et al., Ectopic pregnancy following oral levonorgestrel emergency contraception use, J. Obstet. Gynaecol. Res 45 (2019) 473–476, https://doi.org/10.1111/jog.13815.
[24] J.C. Jacobson, F.E. Likis, P.A. Murphy, Extended and continuous combined contraceptive regimens for menstrual suppression, J. Midwifery Women'S. Heal 57 (2012) 585–592, https://doi.org/10.1111/j.1542-2011.2012.00250.x.
[25] E.G. Raymond, V. Halpern, L.M. Lopez, Pericoital Oral Contraception With Levonorgestrel, Obstet. Gynecol. 117 (2011) 673–681, https://doi.org/10.1097/AOG.0b013e318209dc25.
[26] R.G. Koch, A. Tsamis, A. D'Amore, W.R. Wagner, S.C. Watkins, T.G. Gleason, et al., A custom image-based analysis tool for quantifying elastin and collagen micro-architecture in the wall of the human aorta from multi-photon microscopy, J. Biomech. 47 (2014) 935–943, https://doi.org/10.1016/j.jbiomech.2014.01.027.
[27] J.N. Amajuoyi, M.O. Ilomuanya, B. Oseni, C.P. Azubuike, A. Krestou, D.A. Vorp, et al., Scanning electron microscopy-based quantification of keratin and hyaluronic acid microstructure in electrospun scaffolds, Beni-Suef Univ. J. Basic Appl. Sci. 13 (2024), https://doi.org/10.1186/s43088-024-00539-0.
[28] H.S. Sofi, A. Abdal-hay, S. Ivanovski, Y.S. Zhang, F.A. Sheikh, Electrospun nanofibers for the delivery of active drugs through nasal, oral and vaginal mucosa: Current status and future perspectives, Mater. Sci. Eng. C. 111 (2020) 110756, https://doi.org/10.1016/j.msec.2020.110756.
[29] Y. Duan, L. Kalluri, M. Satpathy, Y. Duan, Effect of electrospinning parameters on the fiber diameter and morphology of PLGA nanofibers, Dent. Oral. Biol. Craniofacial Res (2021) 1–7, https://doi.org/10.31487/j.dobcr.2021.02.04.
[30] Y. Wang, D.-G. Yu, Y. Liu, Y.-N. Liu, Progress of electrospun nanofibrous carriers for modifications to drug release profiles, J. Funct. Biomater. 13 (2022) 289, https://doi.org/10.3390/jfb13040289.
[31] C. Liu, B. Li, H. Du, D. Lv, Y. Zhang, G. Yu, et al., Properties of nanocellulose isolated from corncob residue using sulfuric acid, formic acid, oxidative and mechanical methods, Carbohydr. Polym. 151 (2016) 716–724, https://doi.org/10.1016/j.carbpol.2016.06.025.
[32] A. Medyukhina, N. Vogler, I. Latka, S. Kemper, M. Böhm, B. Dietzek, et al., Automated classification of healthy and keloidal collagen patterns based on processing of SHG images of human skin, J. Biophotonics 4 (2011) 627–636, https://doi.org/10.1002/jbio.201100028.
[33] V. Agrahari, C. Zhang, T. Zhang, W. Li, T.K. Gounev, N.A. Oyler, et al., Hyaluronidase-sensitive nanoparticle templates for triggered release of HIV/AIDS microbicide in vitro, AAPS J. 16 (2014) 181–193, https://doi.org/10.1208/s12248-013-9546-7.
[34] D. Painuly, U. Nisha, S. Arya, J.B. Sangeeth Krishnan, Effect on in-vitro release of individual and dual contraceptive drug loading from gelatin electrospun fibers, J. Drug Deliv. Sci. Technol. 51 (2019) 454–463, https://doi.org/10.1016/j.jddst.2019.03.026.
[35] E. Venugopal, K.S. Sahanand, A. Bhattacharyya, S. Rajendran, Electrospun PCL nanofibers blended with Wattakaka volubilis active phytochemicals for bone and cartilage tissue engineering, Nanomed. Nanotechnol., Biol. Med 21 (2019) 102044, https://doi.org/10.1016/j.nano.2019.102044.
[36] A.A. Conte, K. Sun, X. Hu, V.Z. Beachley, Effects of Fiber Density and Strain Rate on the Mechanical Properties of Electrospun Polycaprolactone Nanofiber Mats, Front Chem. 8 (2020), https://doi.org/10.3389/fchem.2020.00610.
[37] J. Shao, Y. Zheng, M.A.A. Newton, Y. Li, B. Xin, Effect of electric field induced by collector shape on the electrospun jet motion and fiber structure evolution, Fibers Polym. 24 (2023) 3435–3444, https://doi.org/10.1007/s12221-023-00321-6.
[38] U. Stachewicz, F. Modaresifar, R.J. Bailey, T. Peijs, A.H. Barber, Manufacture of void-free electrospun polymer nanofiber composites with optimized mechanical properties, ACS Appl. Mater. Interfaces 4 (2012) 2577–2582, https://doi.org/10.1021/am300235r.
[39] N. Rambabu, S. Panthapulakkal, M. Sain, A.K. Dalai, Production of nanocellulose fibers from pinecone biomass: evaluation and optimization of chemical and mechanical treatment conditions on mechanical properties of nanocellulose films, Ind. Crops Prod. 83 (2016) 746–754, https://doi.org/10.1016/j.indcrop.2015.11.083.
[40] N. Amiraliyan, M. Nouri, M.H. Kish, Electrospinning of silk nanofibers. I. An investigation of nanofiber morphology and process optimization using response surface methodology, Fibers Polym. 10 (2009) 167–176, https://doi.org/10.1007/s12221-009-0167-9.

[41] S.F. Dehghan, F. Golbabaei, B. Maddah, M. Latifi, H. Pezeshk, M. Hasanzadeh, et al., Optimization of electrospinning parameters for polyacrylonitrile-MgO nanofibers applied in air filtration, J. Air Waste Manag. Assoc. 66 (2016) 912–921, https://doi.org/10.1080/10962247.2016.1162228.
[42] D. Weiss, C. Cavinato, A. Gray, A.B. Ramachandra, S. Avril, J.D. Humphrey, et al., Mechanics-driven mechanobiological mechanisms of arterial tortuosity, Sci. Adv. 6 (2020), https://doi.org/10.1126/sciadv.abd3574.
[43] S. Wang, R. Liu, Y. Fu, W.J. Kao, Release mechanisms and applications of drug delivery systems for extended-release, Expert Opin. Drug Deliv. 17 (2020) 1289–1304, https://doi.org/10.1080/17425247.2020.1788541.
[44] G.S. Offeddu, L. Mohee, R.E. Cameron, Scale and structure dependent solute diffusivity within microporous tissue engineering scaffolds, J. Mater. Sci. Mater. Med 31 (2020) 46, https://doi.org/10.1007/s10856-020-06381-x.
[45] G. Gaynanova, L. Vasileva, R. Kashapov, D. Kuznetsova, R. Kushnazarova, A. Tyryshkina, et al., Self-assembling drug formulations with tunable permeability and biodegradability, Molecules 26 (2021) 6786, https://doi.org/10.3390/molecules26226786.
[46] S.Y. Gu, J. Ren, G.J. Vancso, Process optimization and empirical modeling for electrospun polyacrylonitrile (PAN) nanofiber precursor of carbon nanofibers, Eur. Polym. J. 41 (2005) 2559–2568, https://doi.org/10.1016/j.eurpolymj.2005.05.008.
[47] R.B. Mugume, A. Karubanga, M. Kyakula, Impact of addition of banana fibres at varying fibre length and content on mechanical and microstructural properties of concrete, Adv. Civ. Eng. 2021 (2021), https://doi.org/10.1155/2021/9422352.
[48] M.M. Kareem, T. Hodgkinson, M.S. Sanchez, M.J. Dalby, K.E. Tanner, Hybrid core–shell scaffolds for bone tissue engineering, Biomed. Mater. 14 (2019) 025008, https://doi.org/10.1088/1748-605X/aafbf1.
[49] X. Zhang, R. Nakagawa, K.H.K. Chan, M. Kotaki, Mechanical property enhancement of polylactide nanofibers through optimization of molecular weight, electrospinning conditions, and stereocomplexation, Macromolecules 45 (2012) 5494–5500, https://doi.org/10.1021/ma300289z.
[50] A. Doustgani, Optimization of mechanical and structural properties of PVA nanofibers, J. Ind. Text. 46 (2016) 901–913, https://doi.org/10.1177/1528083715601511.
[51] N. Amiri, Z. Rozbeh, T. Afrough, S.A. Sajadi Tabassi, A. Moradi, J. Movaffagh, Optimization of chitosan-gelatin nanofibers production: investigating the effect of solution properties and working parameters on fibers diameter, Bionanoscience 8 (2018) 778–789, https://doi.org/10.1007/s12668-018-0540-5.
[52] Q. Yang, Z. Xie, J. Hu, Y. Liu, Hyaluronic acid nanofiber mats loaded with antimicrobial peptide towards wound dressing applications, Mater. Sci. Eng. C. 128 (2021) 112319, https://doi.org/10.1016/j.msec.2021.112319.
[53] P. Snetkov, K. Zakharova, S. Morozkina, R. Olekhnovich, Hyaluronic acid: the influence of molecular weight and degradable properties of biopolymer, Polym. (Basel) 12 (2020) 1800, https://doi.org/10.3390/polym12081800.
[54] B.O. Fatile, M. Pugh, M. Medraj, Optimization of the electrospun niobium–tungsten oxide nanofibers diameter using response surface methodology, Nanomaterials 11 (2021) 1644, https://doi.org/10.3390/nano11071644.
[55] C.S. Miranda, A.F.G. Silva, S.M.M.A. Pereira-Lima, S.P.G. Costa, N.C. Homem, H. P. Felgueiras, Tunable spun fiber constructs in biomedicine: influence of processing parameters in the fibers' architecture, Pharmaceutics 14 (2022), https://doi.org/10.3390/pharmaceutics14010164.
[56] D. Painuly, U. Nisha, S. Arya, J.B. Sangeeth Krishnan, Effect on in-vitro release of individual and dual contraceptive drug loading from gelatin electrospun fibers, J. Drug Deliv. Sci. Technol. 51 (2019) 454–463, https://doi.org/10.1016/j.jddst.2019.03.026.
[57] S. Lee, S.M. Lee, S.H. Lee, W.K. Choi, S.J. Park, D.Y. Kim, et al., In situ photo-crosslinkable hyaluronic acid-based hydrogel embedded with GHK peptide nanofibers for bioactive wound healing, Acta Biomater. 172 (2023) 159–174, https://doi.org/10.1016/j.actbio.2023.10.011.
[58] P. Boyd, S.M. Fetherston, C.F. McCoy, I. Major, D.J. Murphy, S. Kumar, et al., Matrix and reservoir-type multipurpose vaginal rings for controlled release of dapivirine and levonorgestrel, Int J. Pharm. 511 (2016) 619–629, https://doi.org/10.1016/j.ijpharm.2016.07.051.